Int. J. Microgravity Sci. Appl., 33 (4) (2016) 330407
DOI: 10.15011/jasma.33.330407

IIIII ISPS-6 Proceedings IIIII
(Original Paper)

Improvement of Interference Fringe Analysis for Soret Coefficient Measurement in Soret-Facet Mission

Takuma OSADA[1*], Yoshitaka HASHIMOTO[1], Momoko TOMARU[1], Shinsuke SUZUKI[1]
Yuko INATOMI[2], Yuichi ITO[3] and Taro SHIMAOKA[4]

Abstract

In the Soret-Facet performed on the International Space Station, the Soret coefficient S_T for salol/*tert*-butyl alcohol was measured by using a two-wavelength Mach-Zehnder interferometer. The temperature difference between the sides of the solution was set to 10°C so that its mean temperature was 45°C. The refractive index changes in a narrow observation field were measured by using a charge-coupled device camera. We improved the interference fringe analysis used to determine the refractive index changes by determining the interference fringe shifts in a wide area of the solution rather than in the narrow observation field. The interference fringe shifts outside the observation field were measured by moving the field of view and comparing the interference fringe positions. The fringes were found to shift linearly in the wide area. Then, the values of S_T in the observation field and the wide area, $S_{T\text{narrow}}$ and $S_{T\text{wide}}$, respectively, were determined based on the interference fringe shifts. The measurement error $\delta(S_T)$ was caused by the standard deviation of the slopes of the fit lines, and values of $\delta(S_T)_{\text{narrow}} = \pm 0.34\ \text{K}^{-1}$ and $\delta(S_T)_{\text{wide}} = \pm 0.024\ \text{K}^{-1}$ were obtained for the observation field and the wide area, respectively. Based on the fit lines, which satisfied two constraints, $S_{T\text{narrow}}$ and $S_{T\text{wide}}$ were determined to be -0.17 K^{-1} and -0.06 K^{-1}, respectively, for *tert*-butyl alcohol in salol. Consequently, $\delta(S_T)_{\text{narrow}}/S_{T\text{narrow}} = 190\%$ and $\delta(S_T)_{\text{wide}}/S_{T\text{wide}} = 40\%$ were obtained. Thus, the error $\delta(S_T)/S_T$ decreased from 190% to 40% when the interference fringe shifts were measured in the wide area in 0.25 mm intervals rather than in the narrow observation field.

Keywords: Soret, ISS, Kibo, Salol/*tert*-butyl alcohol, Mach-Zehnder interferometer
Received 30 September 2016, accepted 31 August 2016, published 31 October 2016.

1. Introduction

The mass flux in a solid, liquid, or gas that is caused by a temperature gradient is called the Soret effect. When a temperature gradient is applied to a mixture, a solute in the solution is transported to either the lower- or higher-temperature side of the solution and a solute concentration gradient is established. The Soret effect is important in solute redistribution during the crystal growth of alloys. Therefore, the Soret coefficient S_T, which is the thermodynamic parameter describing the Soret effect, is measured to construct a theoretical model of this effect[1)] and is defined as follows:

$$S_T = -\frac{1}{C_0(1-C_0)}\frac{\nabla C}{\nabla T} \quad (1)$$

Here, C_0 is the initial concentration of the solute, and ∇C and ∇T are the concentration gradient and temperature gradient, respectively. Thus, it is necessary to measure ∇C and ∇T to calculate S_T.

It is difficult to measure S_T under terrestrial conditions because the mass transfer caused by the Soret effect is much smaller than that caused by convection. Therefore, the European Space Agency research team conducted the Influence of Vibrations on Diffusion in Liquids, *IVIDIL*[2)], Diffusion and Soret Coefficients, *DSC*[3)], and SODI-DSC, *DCMIX*[4)] missions on the International Space Station (ISS). In these missions, the influence of *g*-jitter on diffusion and thermodiffusion in liquid was clarified and S_T was measured in binary mixtures by using a one-wavelength Mach-Zehnder interferometer.

Then in the Soret-Facet mission, experiments were performed in the Kibo module on the ISS using a two-wavelength Mach-Zehnder interferometer (2-MZI) to measure S_T for *tert*-butyl alcohol in salol. The advantages of 2-MZI are as follows.

1) Forced convection is absent because the measurement is contactless.
2) Temperature and concentration changes can be measured simultaneously by using two different wavelengths.

However, the interference fringe observation field was quite small, so the data analysis was limited to a small part of the sample solution. The errors of small concentration changes in a limited observation field may cause the error $\delta(S_T)/S_T$ to increase. To solve this problem, we focused on improving the

1 Faculty of Science and Engineering, Waseda University, 3-4-1 Okubo, Shinjuku-ku, Tokyo 169-8555, Japan.
2 Institute of Space and Astronautical Science, Japan Aerospace Exploration Agency, 3-1-1 Yoshinodai, Chuo-ku, Sagamihara, Kanagawa 252-5210, Japan.
3 Human Spaceflight Technology Directorate, Japan Aerospace Exploration Agency, 2-1-1 Sengen, Tsukuba, Ibaraki 305-8505, Japan.
4 Japan Space Forum, Shin-Ochanomizu Urban Trinity Bldg. 2F 3-2-1 Kandasurugadai, Chiyoda-ku, Tokyo 101-0062, Japan.
*E-mail: amukat-adaso@fuji.waseda.jp

interference fringe analysis used to determine the refractive index changes by measuring the fringe shifts in a wide area of the solution, as well as on decreasing $\delta(S_T)/S_T$.

2. Experimental Procedure

2.1 Experimental Apparatus

The Solution Crystallization Observation Facility (SCOF) and its 2-MZI, which had already been set up in Kibo, were used. **Figure 1** shows a schematic illustration of the 2-MZI. Two laser beams with wavelengths of 532 nm and 780 nm were separated into reference and sample beams by a Köster prism. After passing along their optical paths, the laser beams were recombined by a second Köster prism. The interference fringes were observed by a charge-coupled device (CCD) camera (480 × 640 pixels). The size of the observation field was 2.4 × 3.2 mm^2. The two laser beams were alternately turned on and off in 3 s intervals.

The cell in this study was identical to the Facet-Cell[5] that was used in the crystal growth experiment Facet. **Figure 2** shows a schematic illustration of the Facet-Cell ($16^L \times 4.8^W \times 1^T$ mm^3).

Both sides of the cell were heated up to and maintained at 50°C with Peltier devices. Then, the temperature of one side was lowered from 50°C to 40°C. The temperatures of the Peltier devices were measured by thermistors. The obtained temperature history of the Peltier devices is shown in **Fig. 3**.

The center of the observation field was set at a distance X = 9.5 mm from the lower-temperature side; this location was used as the home position. In this mission, the cell was moved to measure the refractive index changes in a wide area of the solution. The beginnings and ends of the periods during which the cell was moved are indicated by the dotted lines in **Fig. 3**, where Period A and Period B correspond to the intervals during which the cell was moved just before setting the temperature gradient and just before the end of the observation time, respectively. During Periods A and B, the view was moved from the home position to the end of the lower-temperature side. Next, it was moved longitudinally from the end of the lower-temperature side to the end of the higher-temperature side, a total distance of 7.1 mm, and images of the interference fringes were taken every 1.6 mm. Next, the view was moved into the field including the thermocouple (TC) to confirm its position. Finally, it was returned to the home position.

Since the S_T measurements were sensitive to vibrations caused by, for example, docking and crew exercise, the Soret-Facet experiments were performed during the crew sleeping time to avoid disturbances due to crew motion. The tri-axial acceleration was measured by the Microgravity Measurement Apparatus. This experiment was performed in the standard microgravity conditions in which research is conducted on the ISS.

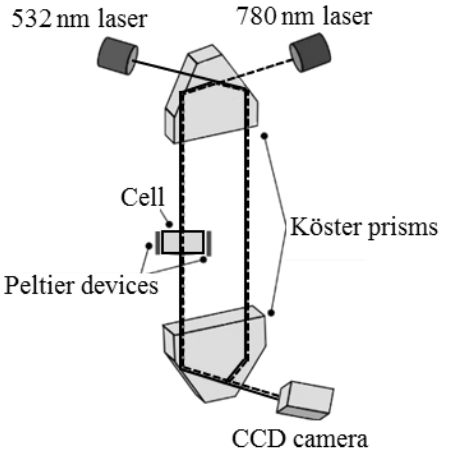

Fig. 1 Two-wavelength Mach-Zehnder interferometer.

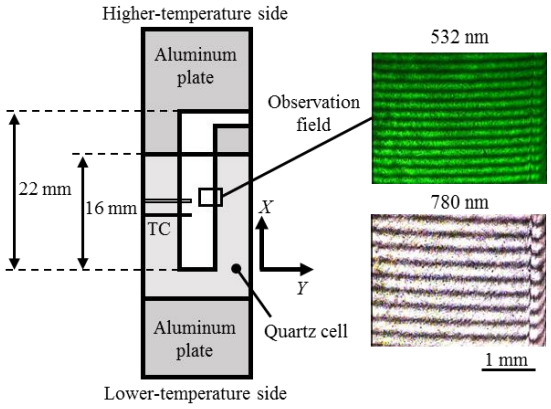

Fig. 2 Schematic illustration of Facet-Cell ($16^L \times 4.8^W \times 1^T$ mm^3) and images of interference fringes (532 nm and 780 nm) in observation field (2.4 × 3.2 mm^2). Sample-filled inlet was set in aluminum plate on higher-temperature side.

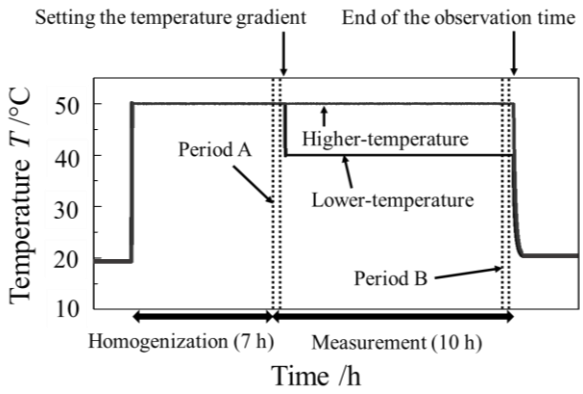

Fig. 3 Obtained temperature history of Peltier devices. Solution was homogenized at 50°C. View was moved during Periods A and B.

2.2 Sample Solution

The Facet-Cell was filled with salol/*tert*-butyl alcohol. Salol, which is commonly used in crystal growth experiments, was selected in this study for the following reasons. First, salol can be melted easily due to its low melting point of 41.5°C, which is slightly higher than room temperature. Second, salol remains in a supercooled liquid state even at temperatures far below the melting point.

The nominal and actual concentrations of *tert*-butyl alcohol may differ because of its high volatility. Therefore, the actual concentration of *tert*-butyl alcohol was measured, using two TCs inserted inside the solution and the equilibrium phase diagram of salol/*tert*-butyl alcohol.

The temperature on the lower-temperature side was set to 27°C, while that on the higher-temperature side was controlled so that only the half of the sample was melted and the solid–liquid interface was near the TCs.

The view was moved longitudinally, and three images were obtained because the observation field was small. The three images were joined together to clarify the position relationships between the two TCs and the solid–liquid interface.

2.3 Analysis Method

The interference fringe shifts Δm were monitored and recorded as movies by the CCD camera to determine the refractive index changes. These movies were saved once in the Image Processing Unit onboard Kibo and were sent to the Tsukuba Space Center of JAXA through NASA's submarine cables.

Using the Δm values of each laser beam, the changes in the temperature ΔT and concentration ΔC were calculated by using Eq. (2), in which the values representing the temperature and concentration dependences of the refractive index that were measured previously have already been inserted[6]:

$$\begin{pmatrix}\Delta T\\ \Delta C\end{pmatrix} = \begin{pmatrix}1.965 & -4.519\\ -1.238 & 1.847\end{pmatrix}\begin{pmatrix}\Delta m_{532}\\ \Delta m_{780}\end{pmatrix} \tag{2}$$

Here, Δm is defined as the number of dark lines that pass through an observation point during the measurement period. The method used to measure this shift is illustrated in **Fig. 4**.

Δm was separated into integer and fraction parts, $Int(\Delta m)$ and $Frac(\Delta m)$, respectively, as follows:

$$\Delta m = Int(\Delta m) + Frac(\Delta m) \tag{3}$$

where

$$\begin{aligned} Frac(\Delta m) &= Frac(\Delta m)_{Period\ B} - Frac(\Delta m)_{Period\ A}\\ &= \left(\frac{\Delta L}{L}\right)_{Period\ B} - \left(\frac{\Delta L}{L}\right)_{Period\ A} \end{aligned} \tag{4}$$

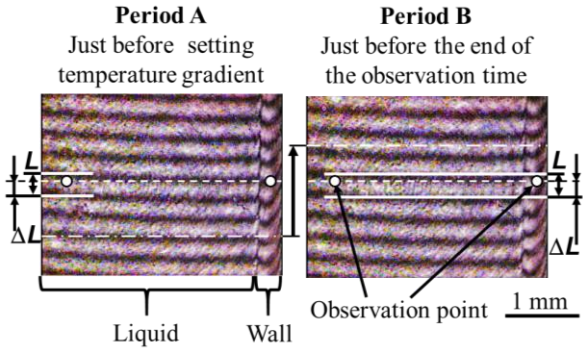

Fig. 4 Example of interference fringe shift observation.

Here, ΔL is the distance between one interference fringe and the observation point, and L is the pitch of the interference fringes. When Δm was measured outside the observation field, $Frac(\Delta m)$ was obtained by comparing the interference fringe positions at times during Periods A and B, while $Int(\Delta m)$ was determined inside the observation field because it was approximately the same outside the field.

The refractive index change of the cell was simultaneously measured to determine its thermal expansion, which could be obtained by subtracting Δm in the cell wall from Δm in the liquid[6].

In the wide area, the refractive index changes were determined by comparing the interference fringe positions at times during Periods A and B, using images obtained in 0.25 mm increments. Then, multiple regression analysis was performed for Δm in the narrow and wide areas, and the standard deviations of the slopes of the fit lines were obtained.

Only the fit lines satisfying the following two constraints within the standard deviation range were employed for further analysis:

1) $\Delta m_{532} > \Delta m_{780}$ in the whole cell;
2) $\Delta C = 0$ in the center of the cell.

The parameters of the fit lines were substituted into Eq. (2), and the gradients of ΔT and ΔC, which were denoted as ∇T and ∇C, respectively, were obtained. Then, S_T was calculated by using Eq. (1). Finally, a reasonable value of S_T was determined at each wavelength by using least-squares analysis to identify the fit line that minimized the residuals.

3. Results and Discussion

3.1 Sample Solution

Figure 5(a) shows the images obtained that include the two TCs and the solid–liquid interface. The solid area was a crystal of salol/*tert*-butyl alcohol. **Figure 5 (b)** indicates the temperature at each position. First, the temperature of the solid–liquid

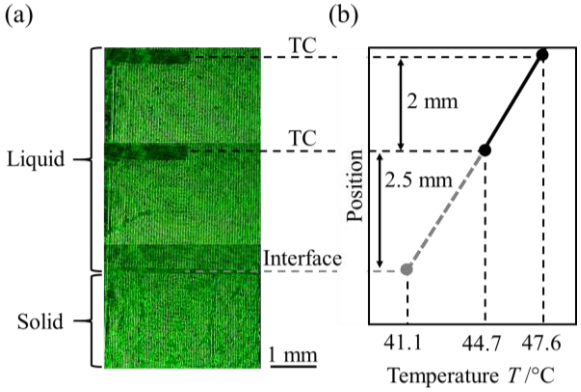

Fig. 5 (a) images and (b) temperatures of two TCs and solid–liquid interface.

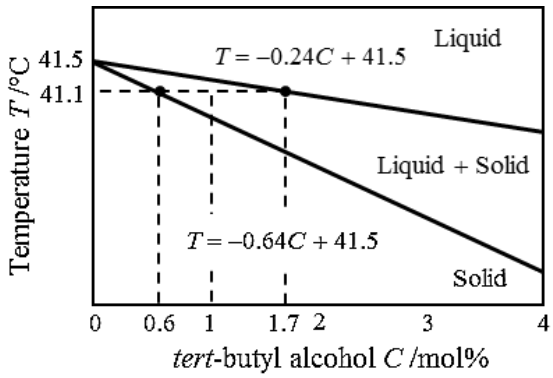

Fig. 6 Equilibrium phase diagram of salol/*tert*-butyl alcohol[7]. Measured temperature (41.1°C) at solid–liquid interface is shown and was used to determine actual *tert*-butyl alcohol concentration.

interface was determined to be 41.1°C by assuming that the temperature distribution was linear and extrapolating the line connecting the points representing the temperatures of the two TCs. Then, this temperature was substituted into the equations of the liquidus and solidus lines in the equilibrium phase diagram[7] depicted in **Fig. 6**. Using this method, the concentration range of *tert*-butyl alcohol was found to be 0.6–1.7mol%. The actual concentration of *tert*-butyl alcohol was assumed to be the average of the endpoints of this range and was thereby determined to be 1.15±0.55mol%.

3.2 Measurement of Fringe Shift in Wide Area

Δm was measured for each laser beam in the observation field, which was the home position. **Figure 7** shows Δm at $X = 9$ mm. It is evident from this figure that the interferometer fringes in the cell wall also shifted because of the refractive index changes caused by the thermal expansion of the quartz plate. Therefore, the thermal expansion of the cell could be calibrated by subtracting "Δm in the cell wall" from "Δm in the liquid + wall."

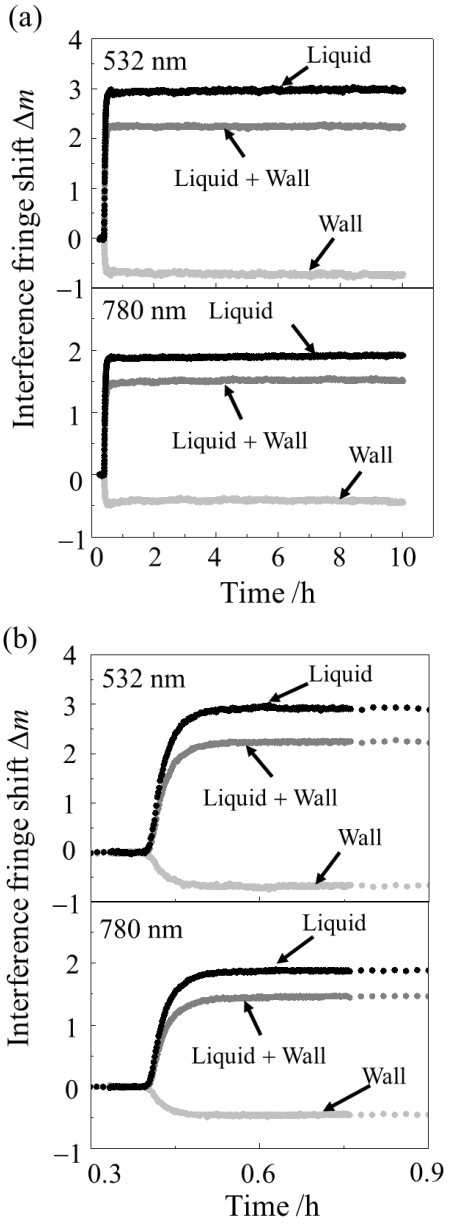

Fig. 7 Δm at $X = 9$ mm versus time (a) from beginning to end of observation time and (b) just after setting temperature gradient.

Next, Δm was measured in the wide area to decrease the S_T error. The results of these measurements are presented in **Fig. 8**. The black rectangle in **Fig. 8** indicates the observation field, and the black and gray symbols correspond to the Δm measurements for the 532 nm and 780 nm laser beams, respectively. It is evident that Δm varies linearly with X for each laser beam.

Next, the linear relationships in the narrow and wide areas were analyzed using multiple regression analysis. The results of this analysis are shown in Table 1 for each laser beam. The fit line in each case was obtained using

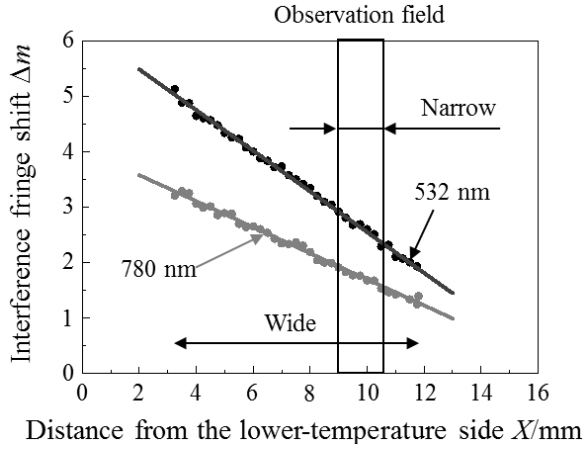

Fig. 8 Δm versus X.

Table 1 Results of multiple regression analysis

Wave length	Area	Gradient A (mm^{-1})	Standard deviation δA(mm^{-1})
532 nm	Narrow	-0.3595	±0.0434
	Wide	-0.3679	±0.0032
780 nm	Narrow	-0.2153	±0.0238
	Wide	-0.2353	±0.0032

$$\Delta m = (A \pm \delta A)X + (B \pm \delta B) \tag{5}$$

Here, A and B are the gradient and y-intercept of the fit line, respectively, and δA and δB are the standard deviations of the gradient and intercept, respectively.

The error in Δm was caused by the image processing procedures, such as gray scaling and thinning. This error caused the standard deviations δA that are listed in **Table 1**. As shown, the values of δA achieved by measuring Δm in the wide area are lower than those obtained by measuring it in the narrow area. Then, $\delta(S_T)$ was calculated by using Eqs. (6) and (7):

$$\delta(S_T) = \frac{-1}{C_0(1-C_0)}\sqrt{\left(\frac{\nabla C}{\nabla T^2}\delta(\nabla T)\right)^2 + \left(\frac{1}{\nabla T}\delta(\nabla C)\right)^2} \tag{6}$$

$$\begin{pmatrix}(\delta(\nabla T))^2\\(\delta(\nabla C))^2\end{pmatrix} = \begin{pmatrix}3.861 & 20.42\\1.533 & 3.411\end{pmatrix}\begin{pmatrix}(\pm\delta A_{532})^2\\(\pm\delta A_{780})^2\end{pmatrix} \tag{7}$$

Here, $\delta(\nabla T)$ and $\delta(\nabla C)$ are the errors of ∇T and ∇C, respectively. $\delta(S_T)$ was caused by $\delta(\nabla T)$ and $\delta(\nabla C)$, which in turn were caused by the δA values listed in **Table 1**. By using Eqs. (6) and (7), $\delta(S_T)_{narrow}$ = ±0.34 K^{-1} and $\delta(S_T)_{wide}$ = ±0.024 K^{-1} were obtained.

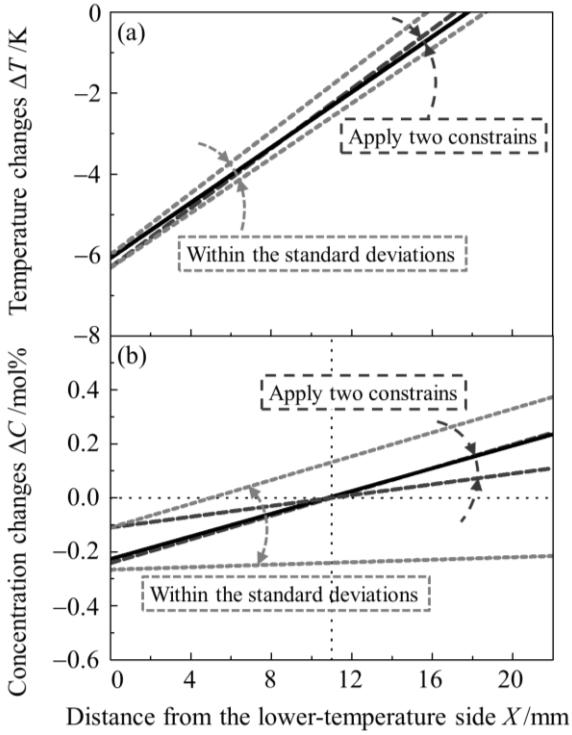

Fig. 9 (a) ΔT versus X and (b) ΔC versus X. Black lines indicate reasonable values of ∇T and ∇C.

3.3 Determination of Soret Coefficient

∇T and ∇C were calculated by substituting the fit line parameters into Eq. (2). As shown in **Fig. 9**, slight changes in A caused large changes in ∇T and, particularly, ∇C.

Then, two constraints were applied to determine reasonable values of ∇T, ∇C, and S_T. However, even with the constraints, there were many possible combinations of ∇T, ∇C, and S_T that could be used to fit the experimental data. Therefore, the residual sums of squares were calculated by using **Fig. 8**, and the relationships between the residual sums of squares and S_T were analyzed. In **Fig. 10**, the gray and black lines indicate the S_T ranges determined based on the fit lines in the observation field and the wide area, respectively. As shown, the S_T range is smaller when Δm was measured in the wide area rather than in the observation field.

The fit lines with the minimum residual sums of squares at each wavelength were those closest to the least-squares fit lines. The parameters of these lines were substituted into Eq. (2) to calculate ∇T and ∇C, which were then employed to calculate reasonable values of $S_{Tnarrow}$ = -0.17 K^{-1} and S_{Twide} = -0.06 K^{-1}.

When distance intervals of 0.25 mm were used, the error $\delta(S_T)_{wide}/S_{Twide}$ was found to be 40%, which is much smaller than $\delta(S_T)_{narrow}/S_{Tnarrow}$ = 190%.

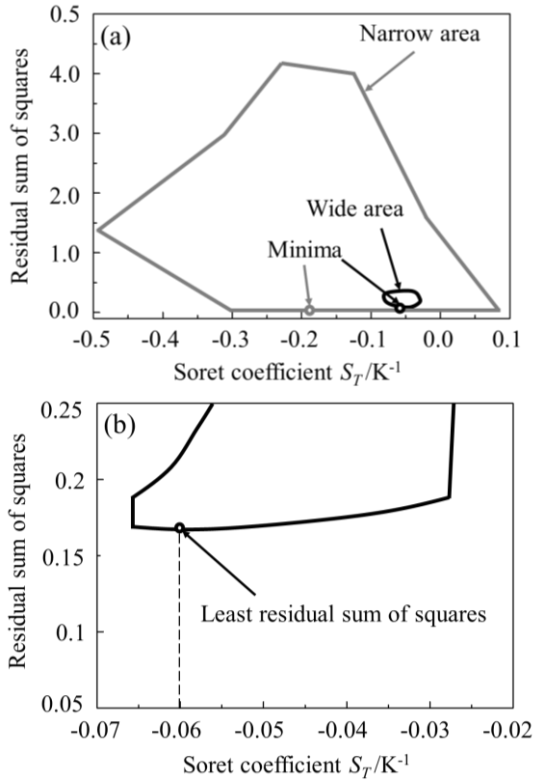

Fig. 10 Residual sum of squares versus S_T: (a) overall view and (b) enlarged view of "wide area."

4. Conclusion

We obtained the following conclusions through this analysis of the Soret-Facet experiment results:

(1) Δm can be measured outside the observation field by moving the view and comparing the interference fringe positions;

(2) The error was improved by 150%, from $\delta(S_T)_{narrow}/S_{Tnarrow}$ = 190% to $\delta(S_T)_{wide}/S_{Twide}$ = 40%, by using observations obtained in a wide area with distance intervals of 0.25 mm rather than those obtained in a narrow area;

(3) S_T was calculated to be -0.06 K^{-1} for *tert*-butyl alcohol in salol when the temperature difference between the two sides of the solution was set to 10°C, so that the mean temperature of the solution was 45°C.

Highly accurate S_T measurements, such as those reported in this paper, will lead to the construction of a more exact theoretical model of the Soret effect.

Acknowledgments

We are grateful to the CIs and UIs of Soret-Facet for the meaningful discussions and the JAXA Flight Control Team (JFCT) and Japan Manned Space Systems Corporation (JAMSS) controlling the payloads during the ISS experiments.

References

1) M.A. Rahman and M.Z. Saghir: Int. J. Heat Mass Transfer, **73** (2014) 693.
2) V. Shevtsova, A. Mialdun, D. Melnikov, I. Ryzhkov, Y. Gaponenko, Z. Saghir, T. Lyubimova and J.C. Legros: C.R. Mecanique, **339** (2011) 310.
3) S. van Vaerenbergh, J.C. Legros, J.L. Daridon, T. Karapantsios, M. Kostoglou and Z.M. Saghir: Microgravity Sci. Technol., **4** (2006) 150.
4) V. Shevtsova, C. Santos, V. Sechenyh, J.C. Legros and A. Mialdun: Microgravity Sci. Technol., **25** (2014) 275.
5) Y. Inatomi, I. Yoshizaki, K. Sakata, T. Shimaoka, T. Sone, T. Tomobe, S. Adachi, S. Yoda and Y. Yoshimura: Defect Diffus. Forum, **323** (2012) 533.
6) Y. Mori, Y. Hashimoto, S. Suzuki and Y. Inatomi: Trans. Jpn. Soc. Aeron. Space Sci., **12** (2014) 37.
7) Y. Inatomi, M. Ashida, K, Sakata and T. Okutani: World J. Eng., **11** (2014) 41.